THERMOGRAPHY APPLIED ON BOUNDARY LAYER TRANSITION VISUALIZATION

Maximilian Kleinubing
Jorge Henrique Bidinotto
Federal University of São Carlos – UFSCar, Rodovia Washington Luís, km 235 - SP-310, 13565-905 – São Carlos – SP, Brazil
bidinotto@ufscar.br

Fernando Martini Catalano
Engineering School of São Carlos – USP, Av. Trabalhador São-carlense, 400, Pq Arnold Schimidt, 13566-590 – São Carlos – SP, Brazil
catalano@sc.usp.br

Eduardo Morgado Belo
Engineering School of São Carlos – USP, Av. Trabalhador São-carlense, 400, Pq Arnold Schimidt, 13566-590 – São Carlos – SP, Brazil
belo@sc.usp.br

Abstract. Aerodynamic laminar flow is of big interest in aeronautical industry, since it produces lower aerodynamic drag, resulting in fuel economy. The determination of this kind of flow around aerodynamic surfaces and its transition to turbulent becomes therefore of great interest for aeronautical design and CFD (Computational Fluid Dynamics) model validation. However such determination presents experimental difficulties, often related with invasive methods, which can influence the flow and the boundary layer of the surface, making the data unrepresentative. This paper presents a methodology for determining the boundary layer transition from laminar to turbulent using high sensitivity infrared cameras. This method relies on the increase of the friction coefficient that occurs during the transition, causing a local increase of temperature that can be detected by these cameras. Its main advantage lies in the fact that it is non-invasive and therefore provides more consistent experimental data, in order to validate theoretical models with better accuracy. The work is based on a theoretical presentation of the methodology and wind tunnel tests conducted at the Laboratory of Aerodynamics of the Engineering School of São Carlos - USP, by members of this institution, together with researchers from EMBRAER S.A. and Federal University of São Carlos - UFSCar.

Keywords: thermography, boundary layer, aerodynamics, infrared

1. INTRODUCTION

During last decades, some aircraft had significant performance benefits using laminar flow over their surfaces for aerodynamic drag reduction. This type of flow can be defined such that fluid flow lines are parallel and without interruption between them.

The transition of the flow from laminar to turbulent has certain peculiarities related mainly to its boundary layer that, due to various factors, may present significant changes in temperature and can therefore be detected by thermal sensors.

This paper presents a proposal for detecting boundary layer transition in flight tests, tested preliminary in wind tunnels with low-speed airfoils, using infrared cameras. The text presents some theoretical concepts, the methodology used and the results of these tests. It is also presented a proposal of possible devices to be used in real aircraft and recommendations for future trials.

2. THEORY

2.1 Infrared technology

Infrared images are generated by processing electro-optical radiation emitted by any object and captured by proper equipment called infrared cameras.

As infrared radiation means the part of the electromagnetic spectrum radiation (Fig. 1) with a wavelength between 0.8 and 1000 microns and are divided into three categories: short infrared radiation (0.8 to 1.5 μm), medium (1.5 to 5.6 μm) and long (5.6 to 1000 μm) as described by Holst (2003).
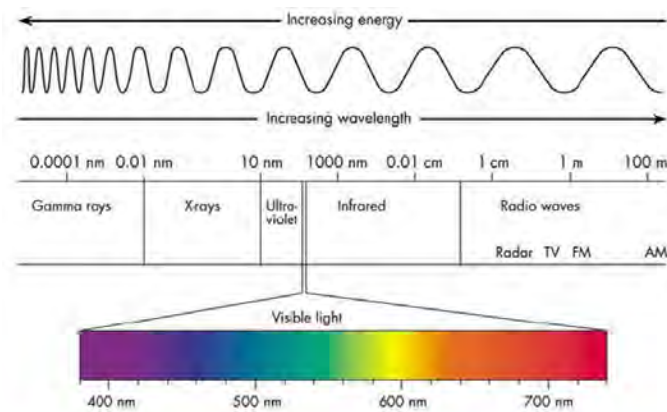
Figure 1. Electromagnetic Spectrum

Thermal radiation is generally in the region of medium infrared radiation (high temperature) or long (low temperature), and this difference in wavelength (and hence frequency) captured by the infrared camera is processed to generate the images based on radiation . Some important features of thermal radiation are:
• All objects emit thermal radiation;
• It does not require a material environment to occur;
• It easily crosses most gases;
• hardly passes through liquids or solids.

In addition to emission an object reacts to the incident radiation environment, absorbing and reflecting a part of it, or allowing a small amount of radiation to cross (such as through a lens). The law of total radiation (W) is derived from this physical principle and can be determined by the following formula:

$$W = \alpha W + \tau W + \rho W \tag{1}$$

Where

$$\alpha + \tau + \rho = 1 \tag{2}$$

The coefficients α, ρ, and τ describe the absorption of incident energy of the object (α), reflection (ρ) and transmission (τ). Each coefficient may have a value between zero and one, depending on the way the object absorbs, reflects or transmits the incident radiation. For example, if $\rho = 0$, $\tau = 0$ and $\alpha = 1$, then there is no energy reflected or transmitted and 100% of the incident radiation is absorbed. That is called a perfect blackbody (Hudson Jr., 1969).

Kirchhoff's law mathematically describes the behavior of bodies with respect to heat. The properties related to the energy irradiation are denoted by the symbol ε, called emissivity of the body. Kirchhoff's law provides that $\alpha = \varepsilon$, either, as both depend on the wavelength, $\alpha(\lambda) = \varepsilon(\lambda)$. Eq. (2) in the case of opaque bodies ($\tau = 0$) can be simplified by:

$$\rho + \varepsilon = 1 \tag{3}$$

In the case of the black body $\rho = 0$ and has therefore $\varepsilon = 1$.

Wyatt (1987) shows that Planck's law given by Eq. (4) describes the amount of energy radiated by a black body in thermal equilibrium and was formulated in 1900 with empirically determined constant. Planck accurately described the blackbody radiation (Fig. 2), suggesting that electromagnetic radiation was emitted in quanta. The Sun is an excellent approximation of a black body (Fig. 3).

$$u(v,T) = \frac{4\pi}{c} I(v,T) = \frac{8\pi h v^3}{c^3} \frac{1}{e^{\frac{hv}{kT}} - 1} \tag{4}$$

Planck assumed that the energy of these oscillations is limited to integer multiples of the fundamental energy E, and proportional to the oscillation frequency n as in Eq. (5). He assumed that quantization theory five years after Albert Einstein have suggested the existence of photons to explain the phenomenon of photoelectric effect.

$$E = hv \tag{5}$$
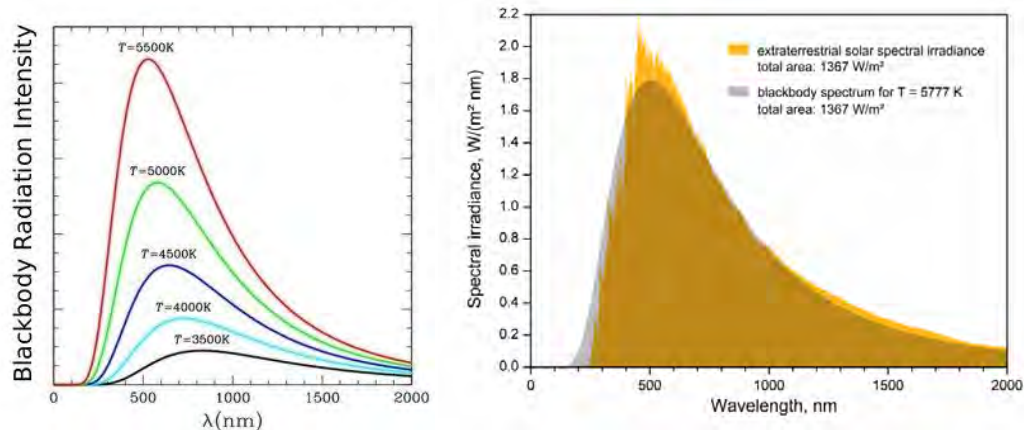
Figure 2. Blackbody radiation and its approximation to the solar irradiance

From Planck's law, the total energy radiated from a blackbody can be calculated. This is expressed by the Stefan-Bolzmann's law:

$$W = \sigma T^4 \tag{6}$$

Where σ is the Stefan-Bolzmann constant (5.67×10^{-8} Wm^{2}K^4) and T is the body temperature.

The properties of radioactive objects are generally described in relation to a perfect blackbody. If the energy emitted from a blackbody is denoted as W_{bb}, and the one of an ordinary object at the same temperature, as W_{obj}, the relationship between these two values describes the emissivity (ε) of the object, as in Eq. (7).

$$\varepsilon = \frac{W_{obj}}{W_{bb}} \tag{7}$$

Consequently, the emissivity is a number between 0 and 1. The better the radioactive properties of the object, the higher its emissivity. An object that has the same emissivity for all wavelengths is called a grey body.

The current infrared cameras can transform the radiation emitted by an object into an image. The infrared radiation is emitted by all objects with a temperature above absolute zero (zero Kelvin) and has similar characteristics to the radiation as a visual reflection, refraction and transmission. The higher the temperature of the body, the greater the radiated energy.

For this reason, the principle of operation of an infrared camera is similar to a light visible wavelength camera. It has a lens which focuses the radiation onto the detector, and a set of electronic hardware and software that processes and samples the generated signals and images.

Therefore, thermography allows one to make temperature measurements of an object without physical contact. Infrared detectors from modern cameras are composed by a focal plane array (FPA) of various materials sensitive to specific wavelength. The sensor resolution array can vary from about 160×120 pixels to 1024×1024 pixels. Depending on the size and resolution of the detectors array it can contain more than 60,000 to 1 million of individual detectors.
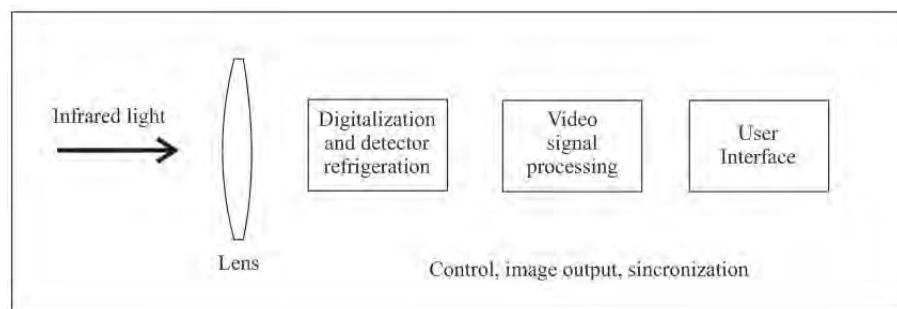
Figure 3. Infrared camera functioning diagram

Also, many cameras manufacturers provide software that allows the cameras to focus on specific areas of the focal plane to calculate the temperature. They have infrared calibration curves that transform the energy radiated by an object being observed into its surface temperature.

The technology of infrared detectors can be divided into two main types: quantum detectors and thermal detectors. A widely used type of thermal detectors uses a microbolometer made of metal or semiconductor material. This type of detector has a lower cost and a broader spectral response when compared to quantum detectors. Microbolometers have slower response (about 12 μs), and are less sensitive than the quantum detectors (about 1 μs).

The quantum detectors are typically made of InSb, InGaAs, PtSi, HgCdTe (MCT) or layers of GaAs/AlGaAs on QWIP detectors (Quantum Well Infrared Photon), quantum detectors that operate based on state change of the electron conducting layer by receiving infrared radiation. These detectors are generally faster and more sensitive than thermal detectors, however, they require cooling. For most demanding applications quantum detectors are usually preferred and operate by taking advantage of the photoelectric principle. These materials absorb photons to raise its electrons to a higher energy level causing a change in conductivity, voltage or current. Reducing the temperature of these detectors to cryogenic levels, they can be very sensitive to infrared radiation while the reaction time to change its energy becomes too small. Cameras using this type of sensors are useful for recording transient events temperature; however, quantum detectors have responses that vary strongly with wavelength, as shown on Fig. 4. Table 1 shows some of the detectors most commonly used today.

Table 1. Types of sensors typically used on infrared cameras

Detector type	Operation	Operation temperature
Microbolometer	High amplitude detector	Non cooled (~30°C)
HgCdTe	Quantum detector for small infrared wavelength	200 K
HgCdTe	Quantum detector for long infrared wavelength	77 K
InSb	Quantum detector for medium infrared wavelength	77 K
PtSi	Quantum detector for medium infrared wavelength	77 K
QWIP	Quantum detector for long infrared wavelength	70 K
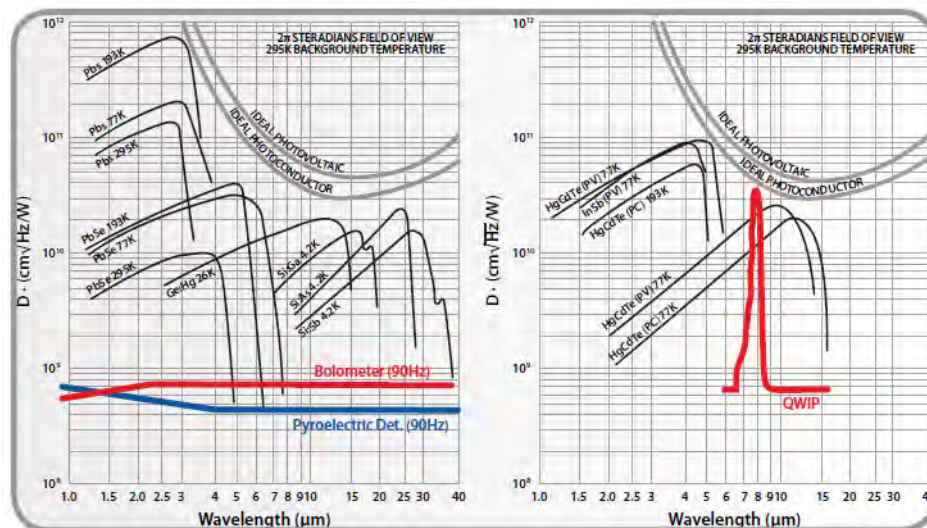
Figure 4. Detectivity curves for different types of detectors. Font: FLIR (2012)

2.2 Boudary layers

When studying aerodynamic viscous flow, apart from the specific viscosity, thermal conductivity effects of this fluid must be considered. These fluid properties acting together, influence each other.

Anderson (1991) makes an analogy between the fluid and various solids sliding one over the other, forming layers, as multiple paper sheets. When you rub this sheet set on a fixed object such as a table top, a phenomenon occurs where the velocity increases as you depart from the fixed object, ie the layer immediately adjacent to the surface has zero velocity, and gradually grows as you move away from this point until it reaches the nominal flow speed. The region close to the surface immersed on the flow, where you can meet this profile with a gradient of velocity, is called boundary layer.

Whereas the flow pressure increases gradually, at a certain time a region with reverse flow will be observed, which generates aerodynamic wake vortices, and the point where this occurs is called aerodynamic separation point, which generates thereafter, the turbulent flow despite of laminar flow observed so far. This phenomenon is illustrated in Fig. 5.
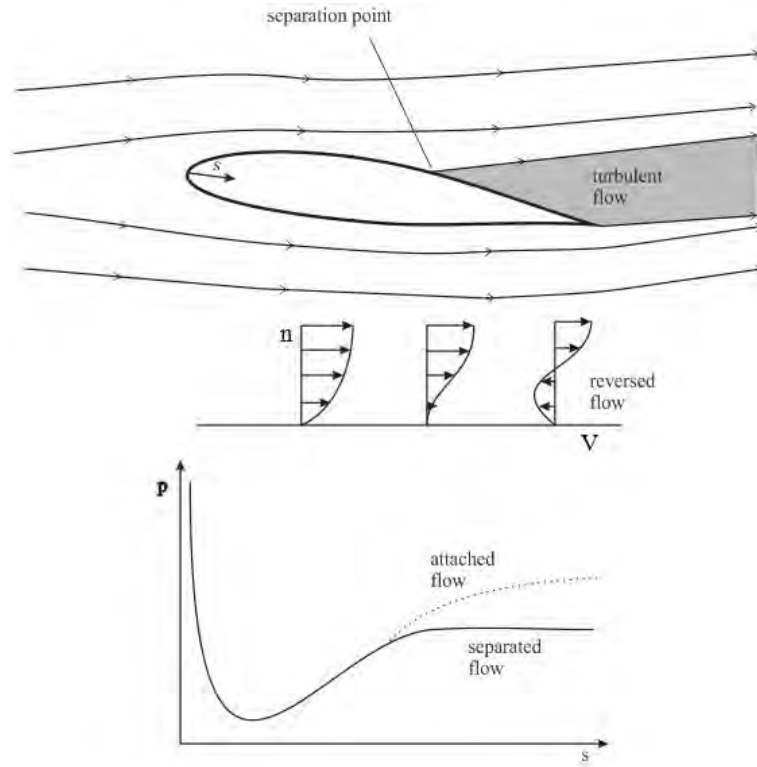
Figure 5. Separation point and its influence on boundary layer and pressure

When the airflow is separated, it becomes turbulent and pressure profile changes dramatically, as shown in the same figure.

A turbulent profile, in turn, has some peculiarities:
- The first relates to the velocity gradient, which is considerably higher in the region close to the surface aerodynamics described on Eq. (8) and graphically on Fig. 6.

$$\left[\left(\frac{\partial V}{\partial n}\right)_{n=0}\right]_{turbulent} > \left[\left(\frac{\partial V}{\partial n}\right)_{n=0}\right]_{la\,min\,ar} \tag{8}$$
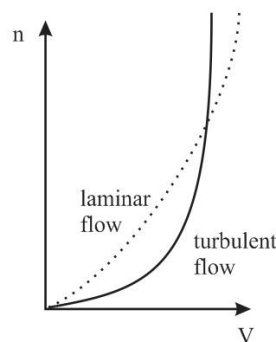
Figure 6. Boundary layer profile on laminar and turbulent flows

- The flow lines are more chaotic in a turbulent flow
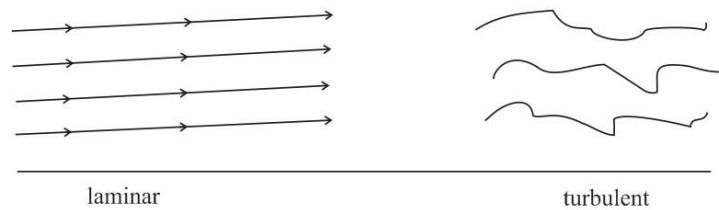
Figure 7. Laminar and turbulent flow lines

- Due to its chaotic profile, turbulent layer is thicker, since, as the surface distance, the flow takes longer to "arrange" and return to have the same velocity than before reaching the surface, as in Fig. 8
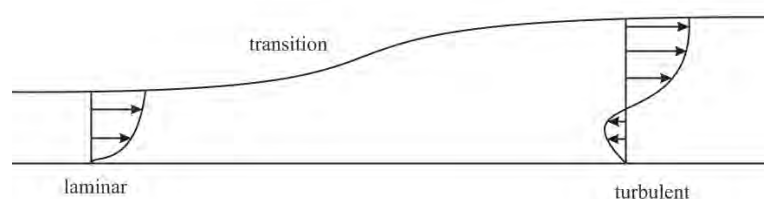
Figure 8. Laminar and turbulent flow thickness

With these considerations, and taking in mind the analogy made earlier in this section, it can be stated that:
1. The generation of heat in a turbulent flow is considerably higher than in a laminar flow, since the friction between irregular "layers" can dissipate more energy in the form of heat.
2. The heat conduction between the aerodynamic surface and the fluid is more effective in a turbulent flow, since the chaotic movement of molecules facilitates a larger number of them to contact the surface, increasing the exchange.

In practical terms, it can be stated that two situations may occur in the case of an air flow on a wing: in the case of a flow hotter than the surface, it can be stated that, based on the first conclusion, above the surface of the wing would be warmer in turbulent flow than in laminar. In the case of a flow colder than the surface of the wing, one can say that its surface must be cooler in turbulent flow, accordingly the second statement above.

Thus, the transition from an aerodynamic flow from laminar to turbulent can be detected by thermal sensors such as infrared imaging cameras

3. METHODOLOGY

Preliminary, wind tunnel tests were performed in order to test the possibility to visualize the boundary layer transition with thermal sensors, and validate the method before applying it in real flight tests.

The tests were performed in the Engineering School of São Carlos – USP, in a small wind tunnel, with open circuit, used for aerodynamic practical lessons.

Two 2D airfoils were tested. The first is a NACA 0012, with 150 mm chord and other a supercritical airfoil, with 100 mm chord. Both were painted in matte black and were exposed to airflow of 28 m/s with around 27 °C of ambient temperature and 5° of angle of attack.

Malerba et al (2008) show that there are two methods to increase the thermal contrast during this kind of test. The first is called 'passive technique', where the air flow is heated before reaching the airfoil, and the second, called 'active technique', where the airfoil surface is heated before the tests.

Because of the wind tunnel configurations, the active technique was chosen, increasing the contrast and getting more satisfactory results, however the first tentative (without heating) did not give good contrasts.

The infrared camera used was a FLIR model P620, and its images were analyzed using the software FLIR QuickReport SP2 v1.2, that made possible a complete analysis, generating temperature measures and changes of some visualization parameters, like temperature range and scales for an image.

After the tests with thermal visualization, both airfoils were tested, in the same conditions as before, with 'flow-viz' (aerodynamic flow visualization with a viscous fluid applied on the airfoil), in order to compare the results and validate the test.

The airfoil NACA 0012 was simulated in software XFLR5 in the same conditions, in order to take more comparative data to validate the tests

4. RESULTS

4.1 Airfoil NACA 0012

Near the airfoil leading edge one vortex generator was positioned to force the transition (see Figure 23) so that one could establish a parameter evaluation for characteristics of the flow profile. Furthermore, along the profile chord, strips of aluminum metal were placed to serve as marks on the infrared images and to help in the analysis of observed outcomes. The first aluminum tape ends at 25% chord and the second starts at 50% chord as shown in Fig. 9.

It is observed in Fig. 10 that the temperature decreases immediately after a disturbance due to an increase in the coefficient of convective heat exchange, which occurs due to increase of the friction coefficient in the turbulent boundary layer. Note also the formation of laminar separation bubble with turbulent reattaching later in the upper region of Fig. 10. At the leading edge the temperature decreases due to the high coefficient of heat exchange by convection, which in this region is due to the small thickness of the boundary layer. Along the flow boundary layer thickness increases, and consequently the coefficient of heat transfer by convection decreases. As a consequence we observe the temperature gradient obtained on the test.

Comparing Fig. 10 with the results obtained with flow-viz shown in Fig. 11, there is a clear similarity in the flow behavior. In both cases there is the formation of laminar separation bubble and transition after the leading edge disturbance in well-defined positions along the string. In a simulation of the NACA 0012 airfoil using the software XFLR5, a transition point from 22% to 5° of angle of attack was obtained, which is very similar to that observed in Fig. 10 and Fig. 11 (using the aluminum tape as reference).
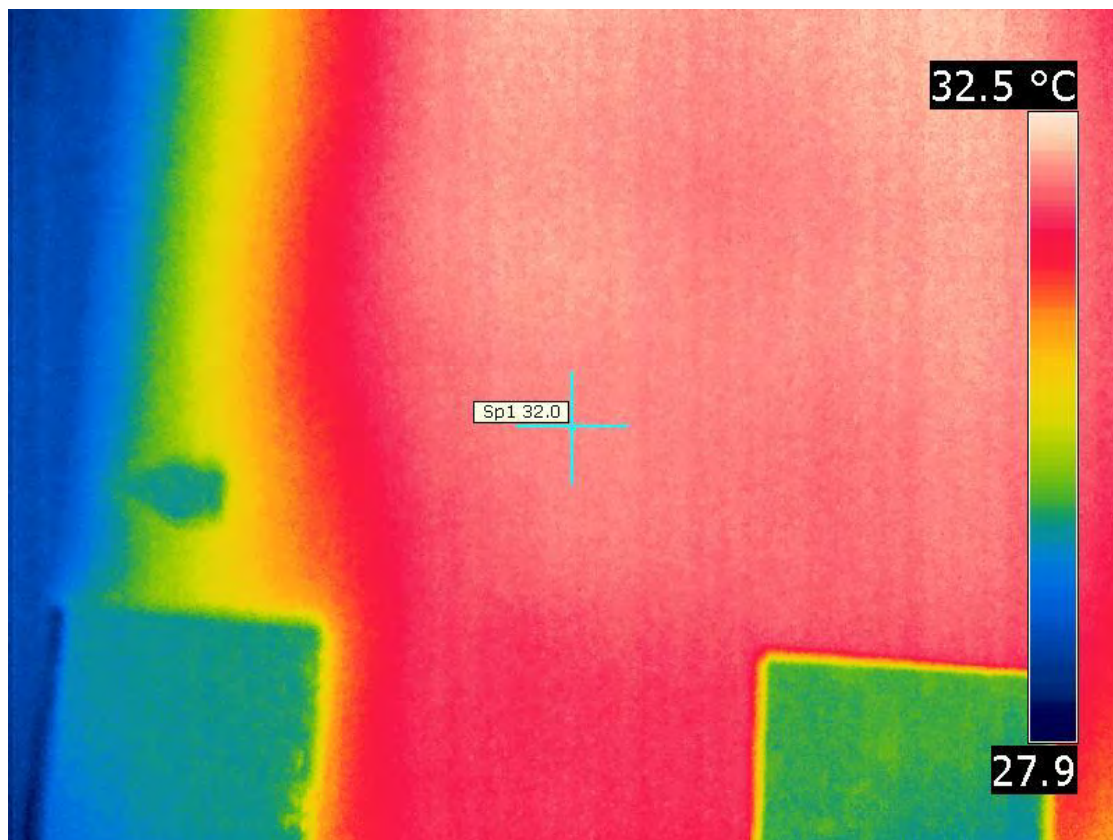
Figure 9. Thermal image of NACA 0012 airfoil before aerodynamic flow

Figure 10. Thermal image of NACA 0012 airfoil exposed to aerodynamic flow (5° angle of attack)

Figure 11. Image of NACA 0012 airfoil during flow-viz visualization (5° angle of attack)

The infrared camera adjustment is one of the important factors for good results. There was some difficulty in focusing the camera because of the short distance between the hole and the tunnel model (about 30 cm). The assumed emissivity was 0.98 (same for human skin) and reflected temperature was assumed equal to the atmospheric temperature. These parameters are configurable after the test using the FLIR QuickReport software v1.2 SP2 (2009).

Using this software it could be seen that the variation in temperature between the leading edge of the laminar profile and the bubble is larger than 2°C during test conditions.

Another relevant fact is that the contrast of heat required to obtain infrared images was obtained by heating the models uniformly before testing in the tunnel. After the start of the air flow, the contrast observed in Fig. 9 to Fig. 10 lasted a certain time (about 5 minutes) after which infrared image became less clear and uniformly colored, which indicates that the heat gradients will decrease and thus hindering the visualization.

4.2 Supercritical airfoil

The same experiment was repeated to an asymmetric airfoil obtaining an image without aerodynamic flow (Fig. 12), an infrared image during air flow at the same conditions (Fig. 13) and as image Flow-Viz (Fig. 14). It is observed that in this case the variations in temperature between the leading edge and the bubble separation is about 4°C.
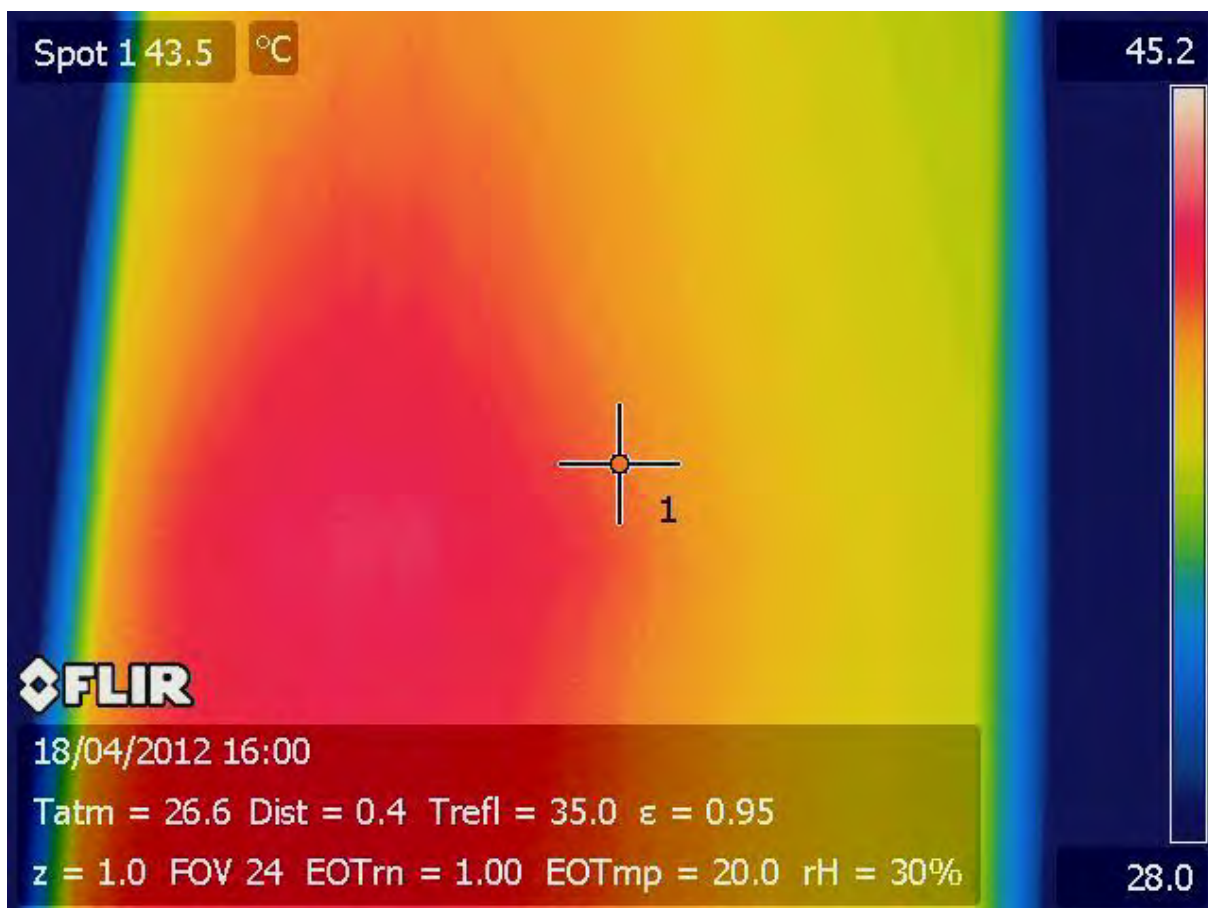
Figure 12. Thermal image of supercritical airfoil before aerodynamic flow

M. Kleinubing, J. H. Bidinotto, F. M. Catalano and E. M. Belo
Thermography Applied on Boundary Layer Transition Visualization
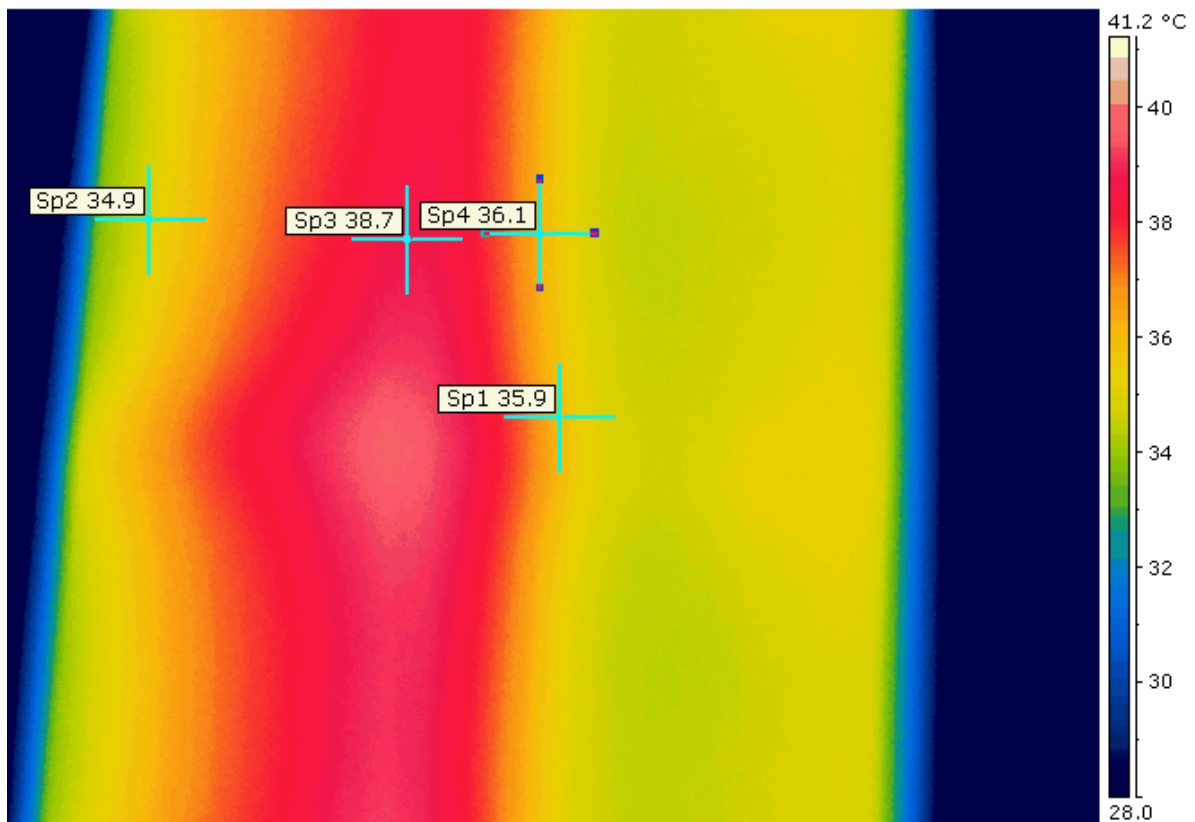
Figure 13. Thermal image of supercritical airfoil exposed to aerodynamic flow (5° angle of attack)

Figure 14. Image of supercritical airfoil during flow-viz visualization (5° angle of attack)

5. CONCLUSIONS AND COMMENTS

Preliminary results show that observation of boundary layer transition with infrared camera provides satisfactory and consistent results in comparison with other visualization method. The wind tunnel tests showed that the method is advantageous for future use in flight test, but some additional difficulties must be overcome, such as:

- Treatment of surface to be investigated with high emissivity paint (preferably matte black, other colors should be investigated).
- Positioning the camera in photo POD or installed on a chase aircraft.
- Possible undesirable thermal effects such as those generated by fuel tanks or other structures or struts installed under the surface of interest.
- The optimal chase aircraft distance or photo POD camera position to make the shoot.
- Choice of aircraft parts that have laminar flow for observation.

Other difficulties still need to be better understood as the best camera setup and data analysis via software. Such problems are under study and will be addressed before their use in actual aircraft.

Other tests should be performed in the future, before flight tests:

- Wind tunnel tests with other color paintings and aeronautical paints.
- Wind tunnel tests with greater sensitivity cameras and high sampling (FLIR SC series refrigerated and high sampling).
- Wind tunnel tests to verify the possibility of aerodynamic separation visualization with higher angles of attack.
- Use of the technique in bigger wind tunnel to achieve higher Reynolds numbers.
- Tests on wind tunnel to check the effects of wake turbulence generated by aerodynamic surfaces and jet turbines are detectable using thermography.

6. ACKNOWLEDGEMENTS

7. REFERENCES

Anderson Jr., J.D., 1991. *Fundamentals of Aerodynamics*. McGraw-Hill, Inc., New York, 2nd edition.
FLIR, 2012. *The Ultimate Infrared Handbook for R&D Professionals*. FLIR AB, Portland.
Holst, G.C.,2003. Electro-*optical Imaging System Performance*. JCD Publishing, Washington, 5th edition.
Hudson Jr., R.D., Infared System Engineering. John Willey & Sons, New York.
Malerba, M., Argento, M., Salviuolo, A., Rossi, G.L., 2008. "A boundary layer inspection on a wing profile through high resolution thermography and numerical methods". *WSEAS Transactions on Fluid Mechanics*, Vol. 3, pp.18-28.
Wyatt, C.L., 1987. *Radiometric System Design*. Macmillan Publishing Co., New York.

8. RESPONSIBILITY NOTICE

The authors are the only responsible for the printed material included in this paper.